forum acusticum 2026
8-12 September · Graz, Austria

Labyrinth Type Gossembrot-Inspired Metamaterial for Low-Frequency Sound Attenuation

Erfan Asgari[1], Rok Prislan[1]

[1]*InnoRenew CoE, UP IAM & UP FAMNIT, University of Primorska, Titov trg 4, Koper, 6000, Slovenia*

This paper is a revised version of the authors' submitted manuscript that was peer-reviewed by at least two anonymous reviewers.

Abstract

Low-frequency sound insulation remains challenging due to the long sound wavelengths, making conventional acoustic materials largely ineffective at low frequencies. This study proposes a novel single-path, space-coiled metamaterial designed for efficient low-frequency sound attenuation. The metamaterial is a 28 mm thick cylinder with a 100 mm diameter, comprising a top cover with an input vent, a bottom cover with an output vent, and a central labyrinthine space-coiled region inspired by the Labyrinth Type Gossembrot. Acoustic waves propagate along a continuous, 1.26 m long path spiraling around an 22 mm diameter central core, with channel widths of 3– 3.5 mm, significantly extending the effective acoustic path. Sound attenuation in the proposed structure is governed by Fabry–Pérot resonances along the single continuous path. Sound transmission loss (STL) was computed in COMSOL Multiphysics considering the impedance tube setup according to ASTM E2611-17, including thermoviscous effects. The metamaterial was fabricated using 3D printing, showing excellent agreement between numerical and experimental results. The first resonance occurs at 132 Hz, demonstrating a substantial shift of the resonance behavior toward the low-frequency range. The proposed metamaterial enables integration into building wall panels to reduce transmitted noise.

Keywords: *Acoustic metamaterials, Sound transmission loss (STL), Low-frequency sound attenuation, Fabry–Pérot resonances, Labyrinth Type Gossembrot-inspired design*

1. Introduction

Acoustic metamaterials are typically thin and lightweight, and can provide effective sound insulation. They can perform better than conventional materials, particular when the size is smaller than the wavelength [1]. Various types of acoustic metamaterials have been proposed, such as membrane-based designs [2], [3], plate-based structures [4], and acoustic black holes (ABHs) [5]. A more recent class, called labyrinthine metamaterials, controls sound by guiding airflow through spiral paths or by combining these paths with different cavities to produce several types of resonances, including Helmholtz [6], multipolar [7], Fano [8], and Fabry–Pérot [9] resonances. By adjusting these resonances, different sound transmission behaviors can be obtained. Previous studies have also presented various base geometries for labyrinthine metamaterials, such as spider web-inspired designs [10], space-coiling structures [11], and combinations of these approaches [12]. These designs are typically produced using advanced manufacturing methods, such as additive manufacturing, which allow the creation of complex structures.

Various acoustic metamaterial concepts have been investigated to improve low-frequency sound insulation performance. In one approach, sector-shaped labyrinthine resonators were introduced and arranged around a circular configuration, and their performance was governed by Fano resonances. In the lowest-frequency scenario, an STL bandwidth was observed in the range of 276 Hz to 380 Hz [13]. In another study, an acoustic insulation ventilated channel (AIVC), consisting of open sections and narrow channels with different lengths, was examined. A sound insulation level exceeding 20 dB was achieved in the frequency range of 500– 1200 Hz [14]. An ultra-open acoustic metamaterial (UOM) unit was also investigated. An STL of 14 dB was reported at 460 Hz; however, the bandwidth was limited to less than 40 Hz, indicating a narrowband performance [15]. Three-dimensional Hilbert fractal acoustic metamaterials (HFAMs) were also proposed. A total thickness of 70 mm and an effective path length of 4480 mm were considered, and the first Fabry–Pérot resonance was observed at 46.3 Hz. A very strong performance in the ultra-low-frequency range was achieved in this design [16]. In another configuration, a coiled-up metamaterial with impedance matching layers was studied. The total thickness was 151 mm, and the first Fabry–Pérot

Corresponding author: rok.prislan@innorenew.eu.

resonance was reported at 2643 Hz [17]. A different design based on a Hilbert space-filling curve pattern was also introduced. The metamaterial consisted of a cubic solid with a side length of 50.8 mm, containing a continuous channel. An effective path length of 812.8 mm and a total thickness of 50.8 mm were reported, and the first Fabry–Pérot resonance occurred at 328 Hz [18]. Furthermore, a third-order ring-curve fractal-maze metamaterial was examined. A total thickness of 280 mm and an effective path length of 1759 mm were reported, and the STL curve showed a peak around 500 Hz [19]. In addition, a cascaded anisotropic spiral structure was studied. The total thickness was 78 mm, and the effective path length reached 229.26 mm. The first Fabry–Pérot resonance was observed at approximately 2400 Hz, and the target frequency range was between 2000 Hz and 2800 Hz [20].

Overall, most of these studies exhibit weak sound insulation performance at low frequencies below 140 Hz or require relatively large structural thicknesses. Moreover, many acoustic insulation solutions are not designed to simultaneously maintain an open airflow pathway, which limits their applicability in ventilation-related systems. Therefore, developing compact labyrinthine metamaterials capable of providing low-frequency sound insulation while preserving airflow remains an important research challenge.

In this study, a novel labyrinthine metamaterial inspired by the Labyrinth Type Gossembrot [21] was designed for low-frequency sound control. The metamaterial operates based on Fabry–Pérot resonances, where acoustic waves reflect back and forth along a single, long, continuous path, producing well-defined resonance behavior in the STL spectrum. The first Fabry–Pérot resonance occurs at 132 Hz. STL was computed using COMSOL Multiphysics with thermoviscous acoustic physics and the impedance tube method following ASTM E2611-17. Experimental impedance tube measurement was also performed to validate the simulation, demonstrating excellent agreement between numerical predictions and laboratory results.

2. Materials and methods

2.1 Design

Figure 1a illustrates the cross-section of the labyrinthine structure inspired by the Labyrinth Type Gossembrot. The design parameters defining the geometry of the metamaterial are defined in Figure 1 and their value provided in Table 1. The design concept is based on drawing seven pairs of concentric circles–$\{C_2, C_3\}, (C_4, C_5), \ldots, (C_{14}, C_{15})\}$–centered on the central circle C_1. Each pair of circles (C_{2i}, C_{2i+1}), where $i \in \{1, 2, \ldots, 6\}$, is separated by a distance $t_1 = 2$ mm, while the last pair (C_{14}, C_{15}) has a spacing of 4 mm. The entire geometry is then divided into five equal sectors by five hypothetical radial lines, d_1, d_2, d_3, d_4, and d_5, all passing through the origin and separated by 72° angles. Around each radial line d_j, where $j = \{1, \ldots, 5\}$, four parallel auxiliary lines are drawn.

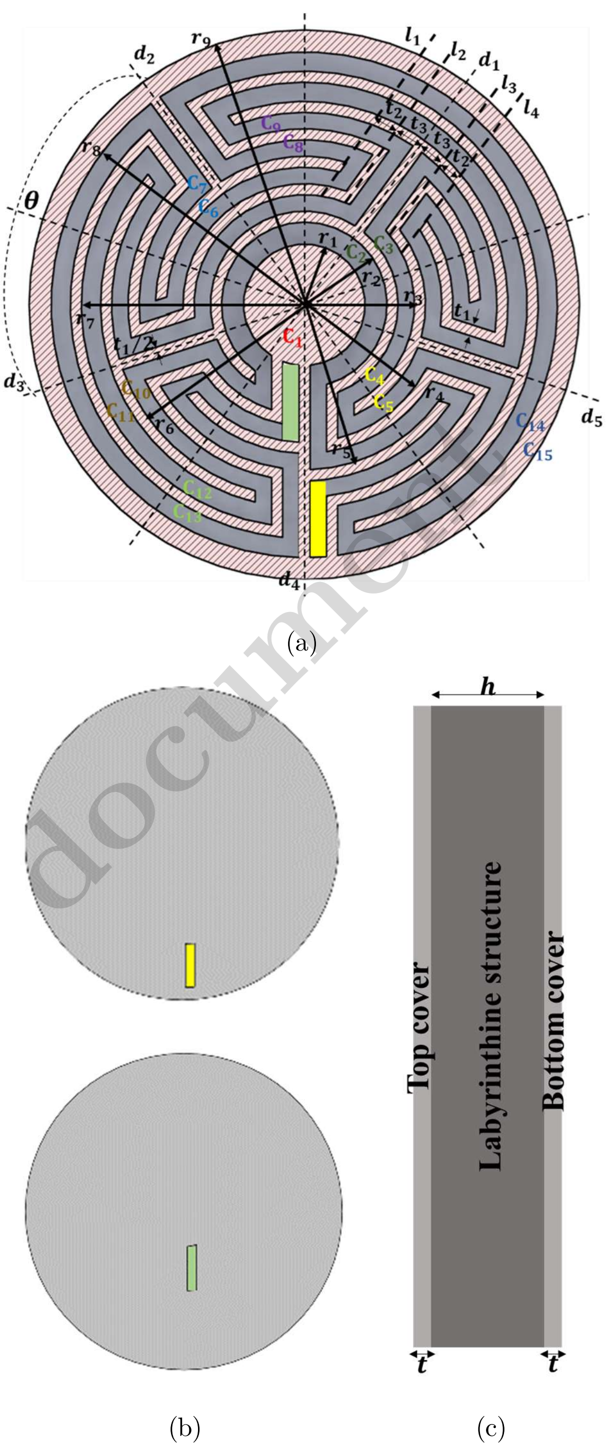

Figure 1. Geometric design and assembly of the Labyrinth Type Gossembrot-inspired metamaterial. (a) Cross-sectional view of the central labyrinthine space-coiled structure. Gray area indicates the air inside the metamaterial. Input and output vents on the top and bottom covers are highlighted in yellow and green, respectively. (b) Top cover with integrated input vent (top) and bottom cover with output vent (bottom). (c) Side view of the fully assembled metamaterial, comprising the top cover, labyrinthine structure, and bottom cover, with total thickness 28 mm (labyrinthine structure 20 mm; each cover 4 mm).

For instance, in the upper-right section of Figure 1a, line d_1 is accompanied by four parallel lines l_1, l_2, l_3, and l_4. The same procedure is applied to d_2, d_3, d_4, and d_5; however, to avoid visual clutter, only the auxiliary lines surrounding d_1 are depicted in the figure. After drawing all auxiliary lines, trimming is performed to remove the overlapping regions between the initial circles and the auxiliary lines, yielding the final Labyrinth Type Gossembrot geometry.

The composition of the designed metamaterial is graphically represented in Figure 1b and Figure 1c. The final metamaterial is assembled by stacking three components: the top cover with an input vent, the labyrinthine structure, and the bottom cover with an output vent. Upon entering the input vent, sound waves propagate through the labyrinthine channels and exit via the output vent, following a single, long, continuous, and unique path. The labyrinthine channels form a complex, space-coiled geometry that considerably extends the effective acoustic path, with an effective path length of $1.26\,\mathrm{m}$ and an overall metamaterial thickness of $28\,\mathrm{mm}$ ($ratio \approx 45$). This extended path significantly enhances low-frequency attenuation. Here, the effective path length is defined as the total distance traveled by acoustic waves along the spiraling channel from the input vent to the output vent.

Table 1. Geometric parameters of the metamaterial structure. All parameters are expressed in mm except the angle θ, which is given in degrees.

$r_1 = 11$	$r_2 = 15$	$r_3 = 20$	$r_4 = 25$	$r_5 = 30$
$r_6 = 35$	$r_7 = 40.5$	$r_8 = 46$	$r_9 = 50$	$t = 4$
$t_1 = 2$	$t_2 = 4$	$t_3 = 5$	$h = 20$	$\theta = 72$

2.2 Manufacturing, simulation, and test

The STL of the metamaterial was evaluated both experimentally and numerically using the impedance tube method in accordance with ASTM E2611-17. For experimental measurements, the STL was determined in the acoustic laboratory at InnoRenew CoE using the B&K Type 4206 Transmission Loss Tube (Figure 2a). The metamaterial sample was manufactured from Polylactic Acid (PLA) using the fused filament fabrication (FFF) additive manufacturing technique. Figure 2b shows the final fabricated sample.

For numerical simulations in COMSOL Multiphysics, the impedance tube was modeled using the acoustic pressure physics module, with the narrow labyrinthine regions inside the metamaterial modeled using thermoviscous acoustics. Given that the acoustic impedance of PLA was significantly higher than that of air, the metamaterial walls were modeled using the Hard Wall boundary condition. A plane wave with an incident pressure amplitude of $1\,\mathrm{Pa}$ was applied at the tube inlet, and a perfectly matched layer (PML) was used at the outlet to mimic an anechoic termination. Physics-controlled mesh was applied for both physics, with the mesh set to "Extremely Fine" and coupled across the two interfaces. The mesh was frequency-dependent, with a maximum frequency of $750\,\mathrm{Hz}$ considered to ensure accuracy across the target range $(100 - 750\,\mathrm{Hz})$.

(a)

(b)

Figure 2. Experimental setup and fabricated sample of the proposed metamaterial. (a) Impedance tube measurement setup. (b) Fabricated metamaterial sample produced using Polylactic Acid (PLA) via fused filament fabrication (FFF): (left) view from the input vent side and (right) view from the output vent side.

The STL of both the fabricated and simulated sample was calculated based on the transfer matrix approach, which relates the sound pressures p and normal particle velocities u at the inlet $(x = 0)$ and outlet $(x = L)$ of a unit layer. The transfer matrix is expressed as [22]:

$$T = \begin{bmatrix} T_{11} & T_{12} \\ T_{21} & T_{22} \end{bmatrix} = \begin{bmatrix} \dfrac{p_L u_L + p_0 u_0}{p_0 u_L + p_L u_0} & \dfrac{p_0^2 - p_L^2}{p_0 u_L + p_L u_0} \\ \dfrac{u_0^2 - u_L^2}{p_0 u_L + p_L u_0} & \dfrac{p_L u_L + p_0 u_0}{p_0 u_L + p_L u_0} \end{bmatrix} \tag{1}$$

where $T_{11}, T_{12}, T_{21}, T_{22}$ are the transfer matrix elements for the layer. Based on this, the transmission coefficient (τ) and the STL were obtained using:

$$\tau = \frac{2e^{ikL}}{T_{11} + T_{12}/\rho_0 c_0 + \rho_0 c_0 T_{21} + T_{22}} \Rightarrow STL = 20\,log_{10}\left|\frac{1}{\tau}\right| \tag{2}$$

where $k = 2\pi f / c_0$ is the wave number, f is the frequency, $\rho_0 = 1.29\,\mathrm{kg/m^3}$ is the air density, and $c_0 = 340\,\mathrm{m/s}$ is the speed of sound in air.

3. Results and Discussion

The acoustic performance of the proposed metamaterial was evaluated in terms of the STL obtained from numerical simulations and experimental measurements (Figure 3). A very high level of agreement is observed between the numerical and experimental results, confirming the accuracy of the simulation approach and the reliability of the fabrication process. The general magnitude of the STL values is well matched in both cases, and the sequence of dips and peaks is preserved, confirming that the periodic resonance behavior of the metamaterial is accurately captured by the numerical model. A detailed comparison indicates that the deviations remain small at low and medium frequencies, while the largest difference, reaching about 4 to 5 dB, appears above 600 Hz. In addition, a slight shift in the resonance positions becomes more noticeable at higher frequencies, where the experimental dips and peaks are observed at slightly different frequencies than those predicted numerically. This behavior is likely related to the higher sensitivity of the higher-order resonances to small fabrication tolerances, surface roughness, and minor uncertainties in the material and boundary conditions.

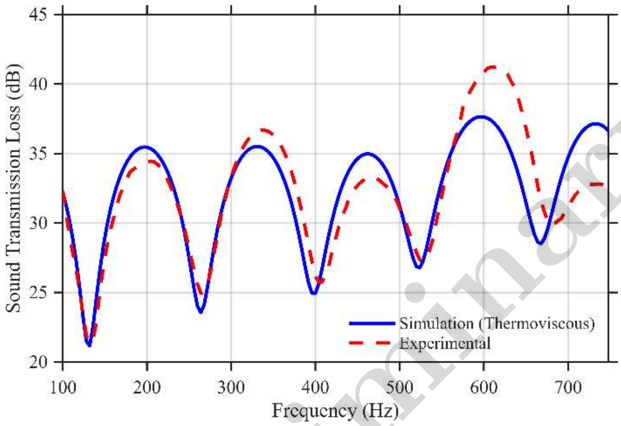

Figure 3. STL as a function of frequency for the proposed acoustic metamaterial, comparing thermoviscous simulation results with experimental measurements.

The STL response exhibits a series of well-defined resonance features associated with Fabry–Pérot resonances along the single, continuous labyrinthine path. This behavior arises from the unique geometric characteristic of the metamaterial, where acoustic waves are constrained to propagate through a single, extended, and continuous channel without any alternative or interfering paths. As a result, the system can be effectively approximated as a one-dimensional acoustic waveguide.

From a physical perspective, the structure behaves as an open–open resonant system, since both the input and output vents are connected to the surrounding medium. In such systems, the resonance frequencies are inversely related to the effective acoustic path length [23]. Therefore, the significantly extended path length in the proposed design leads to a pronounced shift of the resonance frequencies toward the low-frequency range. This effect enables the first resonance to occur at 132 Hz, followed by higher-order resonances at approximately 263 Hz, 398 Hz, 523 Hz, and 667 Hz. At the resonance frequencies, the STL reaches local minima. This behavior can be explained by the formation of standing wave patterns inside the labyrinthine channel, where pressure transmission through the structure is enhanced due to constructive coupling between the incident and transmitted waves. As a result, acoustic energy is more efficiently transmitted across the metamaterial at resonance, leading to reduced transmission loss. Between successive resonances, the STL increases and reaches local maxima, corresponding to anti-resonance conditions where wave transmission is suppressed. Therefore, Fabry–Pérot resonances are shifted toward lower frequencies, which consequently brings the corresponding anti-resonance peaks to lower frequency ranges as well. This shift enables the metamaterial to exhibit effective sound insulation in the low-frequency region.

As discussed previously, the proposed labyrinthine metamaterial can be considered as an open–open acoustic waveguide, where the resonance frequencies are determined by the standing-wave modes established along the extended acoustic pathway. Therefore, the Fabry–Pérot resonance frequencies can be estimated using the following analytical relation [23]:

$$f_n = n c_0 / 2 L_{eff} \tag{3}$$

where f_n represents the frequency of the n-th order Fabry–Pérot resonance. This equation provides a simple estimation of the resonance positions associated with the standing-wave modes inside the coiled pathway and demonstrates the fundamental role of the extended acoustic length in controlling the low-frequency response of the metamaterial.

The Fabry–Pérot resonance frequencies obtained from FEM simulation, experimental measurements, and the analytical prediction using Equation (3) are compared in Table 2. The relative errors between these approaches are also included to quantify their agreement. The close correspondence between the three datasets confirms that the dominant mechanism governing the resonance locations is accurately captured by the effective path length model.

Table 2. Comparison of Fabry–Pérot resonance frequencies obtained from FEM simulation, experimental measurements, and analytical prediction.

Mode	FEM (Hz)	Exp (Hz)	Analytical (Hz)	FEM–Analytical (%)	Exp–Analytical (%)	FEM–Exp (%)
1st	132	132	134.8	2.1	2.1	0.0
2nd	263	264	269.6	2.5	2.1	0.4
3rd	398	406	404.4	1.6	0.4	2.0
4th	523	526	539.3	3.1	2.5	0.6
5th	667	682	674.1	1.1	1.2	2.3

The excellent agreement among the analytical prediction, FEM simulation, and experimental measurements confirms that the effective acoustic path length plays the primary role in determining the Fabry–Pérot resonance positions. However, the other geometrical parameters mainly influence the strength and spectral characteristics of the attenuation response. In particular, the inlet and outlet vent dimensions affect the acoustic impedance and the coupling between the external acoustic field and the internal labyrinthine pathway. Reducing the vent cross-sectional area increases the impedance mismatch, which can modify the transmission amplitude, resonance sharpness, and bandwidth of the STL response. Similarly, the cross-sectional dimensions of the labyrinthine channels influence viscous and thermal losses, acoustic damping, and the quality factor of the resonant modes.

The main objective of this design is therefore not the resonance itself, but the relocation of high-STL regions to lower frequencies within a compact structure. Compared to the studies discussed in the Introduction, where effective sound insulation is often achieved at higher frequencies or requires relatively large structural thicknesses, the proposed design achieves comparable low-frequency performance while maintaining a compact geometry and a significantly extended effective path length.

4. Conclusion

A compact acoustic metamaterial based on a single-path, space-coiled labyrinthine design inspired by the Labyrinth Type Gossembrot was presented for low-frequency sound insulation. The structure comprises three main components: a top cover with an input vent, a central labyrinthine region, and a bottom cover with an output vent. Acoustic waves enter through the input vent on the top cover, propagate along the single, continuous, and extended labyrinthine path, and exit through the output vent on the bottom cover. This open–open configuration enables Fabry–Pérot resonances to dominate the acoustic response along the single path. By constraining sound waves to propagate along a long continuous path within a limited thickness, the effective acoustic length is significantly increased, shifting the entire resonance pattern toward lower frequencies. As a result, not only the Fabry–Pérot resonances but also the corresponding anti-resonance peaks are moved to lower frequencies, enabling effective sound insulation in the low-frequency range within a compact structure. The acoustic performance was evaluated by calculating the STL using both thermoviscous simulations in COMSOL Multiphysics and impedance tube measurements according to ASTM E2611-17. Excellent agreement was observed between simulation and experimental STL results. Overall, the proposed metamaterial demonstrates that efficient low-frequency sound insulation can be achieved using a compact, single-path labyrinthine structure. The combination of a long effective acoustic path, simple geometry, and reproducible STL performance highlights its potential for practical applications in noise control, particularly in HVAC systems, automotive silencers, and building acoustics.
In future work, the proposed unit cell can be arranged into a two-dimensional periodic array on supporting structures, forming modular panels suitable for integration as building walls or window inserts. By opening the central cavity, controlled interactions between different acoustic paths can be introduced, leading to the emergence of additional resonances, including Fano-type resonances, and thus producing richer and more versatile STL spectra. Furthermore, the proposed metamaterial model can be coupled with surrogate modeling and optimization techniques to efficiently enhance STL performance across targeted frequency ranges.

5. Acknowledgments

Authors gratefully thank and acknowledge funding from the EU under the Horizon Europe research and innovation programme through the WoodStock project (Grant Agreement No. 101181021).

References

[1] N. Gao, Z. Zhang, J. Deng, X. Guo, B. Cheng, and H. Hou, "Acoustic Metamaterials for Noise Reduction: A Review," *Adv. Mater. Technol.*, vol. 7, no. 6, p. 2100698, Jun. 2022, doi: 10.1002/admt.202100698.

[2] Z. Yang, J. Mei, M. Yang, N. H. Chan, and P. Sheng, "Membrane-Type Acoustic Metamaterial with Negative Dynamic Mass," *Phys. Rev. Lett.*, vol. 101, no. 20, p. 204301, Nov. 2008, doi: 10.1103/PhysRevLett.101.204301.

[3] E. Asgari, R. Hedayati, A. Ohadi, M. S. Naeini, and M. T. Esfahani, "Prediction, analysis, and improvement of sound insulation performance of membrane-type acoustic metamaterials using machine learning and preliminary experiments," *Appl. Acoust.*, vol. 254, p. 111428, Dec. 2026, doi: 10.1016/j.apacoust.2026.111428.

[4] J. Li, X. Fan, and F. Li, "Numerical and experimental study of a sandwich-like metamaterial plate for vibration suppression," *Compos. Struct.*, vol. 238, p. 111969, Apr. 2020, doi: 10.1016/j.compstruct.2020.111969.

[5] A. Pelat, F. Gautier, S. C. Conlon, and F. Semperlotti, "The acoustic black hole: A review of theory and applications," *J. Sound Vib.*, vol. 476, p. 115316, Jun. 2020, doi: 10.1016/j.jsv.2020.115316.

[6] X. Yang *et al.*, "Development of Adjustable Parallel Helmholtz Acoustic Metamaterial for

Broad Low-Frequency Sound Absorption Band," *Materials*, vol. 15, no. 17, p. 5938, Aug. 2022, doi: 10.3390/ma15175938.

[7] C. Liu, B. Xia, and D. Yu, "The spiral-labyrinthine acoustic metamaterial by coiling up space," *Phys. Lett. A*, vol. 381, no. 36, pp. 3112–3118, Sep. 2017, doi: 10.1016/j.physleta.2017.07.041.

[8] X. Li, H. Zhang, H. Tian, Y. Huang, and L. Wang, "Frequency-tunable sound insulation via a reconfigurable and ventilated acoustic metamaterial," *J. Phys. Appl. Phys.*, vol. 55, no. 49, p. 495108, Dec. 2022, doi: 10.1088/1361-6463/ac9985.

[9] X. Man, B. Xia, Z. Luo, and J. Liu, "3D Hilbert fractal acoustic metamaterials: low-frequency and multi-band sound insulation," *J. Phys. Appl. Phys.*, vol. 52, no. 19, p. 195302, May 2019, doi: 10.1088/1361-6463/ab092a.

[10] G. Y. Song, Q. Cheng, B. Huang, H. Y. Dong, and T. J. Cui, "Broadband fractal acoustic metamaterials for low-frequency sound attenuation," *Appl. Phys. Lett.*, vol. 109, no. 13, p. 131901, Sep. 2016, doi: 10.1063/1.4963347.

[11] Y. Li, B. Liang, X. Zou, and J. Cheng, "Extraordinary acoustic transmission through ultrathin acoustic metamaterials by coiling up space," *Appl. Phys. Lett.*, vol. 103, no. 6, p. 063509, Aug. 2013, doi: 10.1063/1.4817925.

[12] Y. Liu *et al.*, "Sound regulation of coupled Helmholtz and Fabry-Pérot resonances in labyrinth cavity structures," *Ultrasonics*, vol. 95, pp. 45–51, May 2019, doi: 10.1016/j.ultras.2019.03.007.

[13] E. Asgari, A. Ohadi, and R. Hedayati, "Multiple broad bandgaps soundproofing for sectoral labyrinthine metamaterials," *Extreme Mech. Lett.*, vol. 77, p. 102349, Jun. 2025, doi: 10.1016/j.eml.2025.102349.

[14] Z. Su, Y. Zhu, S. Gao, H. Luo, and H. Zhang, "High-Efficient and Broadband Acoustic Insulation in a Ventilated Channel With Acoustic Metamaterials," *Front. Mech. Eng.*, vol. 8, p. 857788, May 2022, doi: 10.3389/fmech.2022.857788.

[15] R. Ghaffarivardavagh, J. Nikolajczyk, S. Anderson, and X. Zhang, "Ultra-open acoustic metamaterial silencer based on Fano-like interference," *Phys. Rev. B*, vol. 99, no. 2, p. 024302, Jan. 2019, doi: 10.1103/PhysRevB.99.024302.

[16] X. Man, B. Xia, Z. Luo, and J. Liu, "3D Hilbert fractal acoustic metamaterials: low-frequency and multi-band sound insulation," *J. Phys. Appl. Phys.*, vol. 52, no. 19, p. 195302, May 2019, doi: 10.1088/1361-6463/ab092a.

[17] X. Jia, Y. Li, Y. Zhou, M. Hong, and M. Yan, "Wide bandwidth acoustic transmission via coiled-up metamaterial with impedance matching layers," *Sci. China Phys. Mech. Astron.*, vol. 62, no. 6, p. 964311, Jun. 2019, doi: 10.1007/s11433-018-9365-6.

[18] G. Comandini, M. Ouisse, V. P. Ting, and F. Scarpa, "Acoustic transmission loss in Hilbert fractal metamaterials," *Sci. Rep.*, vol. 13, no. 1, p. 19058, Nov. 2023, doi: 10.1038/s41598-023-43646-1.

[19] J. Wang, Y. Sun, Y. Wang, Y. Li, and X. Gu, "Design and Characterization of Ring-Curve Fractal-Maze Acoustic Metamaterials for Deep-Subwavelength Broadband Sound Insulation," *Materials*, vol. 18, no. 15, p. 3616, Jul. 2025, doi: 10.3390/ma18153616.

[20] Y. Zhou, "Visco-thermal Effects on Anisotropic and Isotropic Labyrinthine Acoustic Metamaterials in the Cascade," *J. Vib. Eng. Technol.*, vol. 12, no. 1, pp. 223–232, Jan. 2024, doi: 10.1007/s42417-022-00839-8.

[21] H. 1941-1985 Kern, *Through the labyrinth: designs and meanings over 5000 years*. Munich London New York: Prestel, 2000.

[22] A. International, "ASTM E2611-09 Standard Test Method for Measurement of Normal Incidence Sound Transmission of Acoustical Materials Based on the Transfer Matrix Method," ASTM, 2009.

[23] L. E. Kinsler, A. R. Frey, A. B. Coppens, and J. V. Sanders, *Fundamentals of Acoustics*. John Wiley & Sons, 2000.